

Chapter 2

Optical Manipulation of Light Scattering in Cold Atomic Rubidium

1 R. G. Olave*, A. L. Win, K. Kemp, S. J. Roof, S. Balik, and M. D. Havey
2 *Old Dominion University, Department of Physics, Norfolk, Virginia 23529*

3 I. M. Sokolov^{1,2} and D. V. Kupriyanov¹

4 ¹*Department of Theoretical Physics, State Polytechnic University, 195251,*
5 *St.-Petersburg, Russia*

6 ²*Institute for Analytical Instrumentation, RAS, 198103, St.-Petersburg, Russia*

7 A brief perspective on light scattering in dense and cold atomic rubidium is presented. We particularly focus on the influence of auxiliary applied fields on the system response to a weak and nearly resonant probe field. Auxiliary fields can strongly disturb light propagation; in addition to the steady state case, dynamically interesting effects appear clearly in both the time domain, and in the optical polarization dependence of the processes. Following a general introduction, two examples of features found in such studies are presented. These include nonlinear optical effects in (a) comparative studies of forward- and fluorescence-configuration scattering under combined excitation of a control and probe field, and (b) manipulation of the spatial structure of the optical response due to a light shifting strong applied field.

18 1. Introduction

19 The research presented in this chapter forms one part of the broad interface
20 between atomic and condensed matter physics. A particular focus is an overview
21 of quantum optics in high-density and cold atomic matter, in which disorder-driven
22 electromagnetic interactions can develop strongly correlated character.¹ These
23 emergent effects are typified by Anderson localization of light, the onset of random
24 lasing and collective interatomic interactions such as super and sub radiance involving the system particles as a whole. The overriding theme is then

*rolave@odu.edu

1 investigation of the physics of strongly correlated atomic-radiative systems, includ-
2 ing the collective properties and phase transitions in ultracold atomic vapor. A
3 closely related secondary theme appears when we consider the resonant interpar-
4 ticle interactions among the system constituents. Then the macroscopic opti-
5 cal response is modified from the microscopic single atom Lorentzian response
6 to include so-called local field shifts, including the collective Lamb shift^{2,3}. It
7 is important to note that much of the phenomenology appears most strongly in
8 high density gases at low temperatures. By this we mean that the temperatures
9 on the order of 100 μK or less, and atomic densities are characteristically
10 greater than 10^{13} atoms/cm³. For such densities there are typically several
11 atoms in a volume $(\lambda/2\pi)^3$, where λ is the wavelength of light in the atomic
12 medium.

13 We generally emphasize that the processes of emission and absorption of radi-
14 ation in dense gases are quite representative of near-resonant many body interac-
15 tions among the fields and the atoms in the ensemble.^{2,3} In the approximation
16 where the atoms have a pairwise interaction of the dipole type, there contributes
17 both a long range radiative interaction decreasing as $1/r$ with increasing atom-
18 atom separation r , and short range interactions of the form of the Coulomb elec-
19 trostatic dipole-dipole interaction inextricably dipole-dipole interaction. Among
20 other effects which appear when virtual photons are exchanged among the differ-
21 ent atoms in the system there emerges a collective Lamb shift which is essential to
22 description of the global response of the system. In general, the collective aspects
23 yield a modification of the well-known local field shift^{4,5} of the resonance frequency,⁶
24 and (with proper state preparation) an associated superradiant emission from the
25 system.^{7,8}

26 In this chapter we focus on the interaction of a weak and near resonance probe
27 beam with an ensemble of cold atoms. Even more specifically, we consider the
28 influence of a second auxiliary field on the optical response of the probe. Overall,
29 we study influence of auxiliary fields in both the time domain and the dependence
30 on the polarization of both detected light and the relative optical polarization of
31 the auxiliary and probe fields. There are two cases we consider. In the first, the
32 spectral structure of the atomic susceptibility is modified by the auxiliary field.
33 This is the case for the reported experimental results, and associated theoretical
34 calculations, on polarized fluorescence excited in the so called lambda configuration
35 characteristically employed in studies of electromagnetically induced transparency.
36 In the second, we consider modification of the spatial properties of an ultracold
37 ensemble by an auxiliary field which produces a spatially varying light shift of the
38 atomic levels. This approach allows simulation of a quasi one dimensional spatial
39 configuration of atoms which, for instance, can have applications to studies of super-
40 radiance,⁹ Anderson localization¹⁰ of light and random lasing¹¹⁻¹⁴ in reduced spatial
41 geometry.

1 2. Illustrative Topics

2 2.1. Polarized fluorescence studies under conditions of electromag- 3 netically induced transparency in cold atomic rubidium

4 2.1.1. Introduction

5 In this portion of the chapter we report on a primarily experimental study directed
6 towards optical control of weak localization^{15–19} in ultracold atomic vapor. Gen-
7 erally, control is achieved by application of a dressing field to the atomic medium
8 in the presence of the weaker probe incident radiation.^{20,21} Such a configuration
9 has a wide range of applications^{20,22–26,30,31} in nonlinear optics,^{26–29} quantum infor-
10 mation,^{20,22,23} single photon manipulation,^{20,22,23} and precision magnetometry.^{30,31}
11 Here we consider manipulation of the weak probe beam and light scattered from it,
12 thus undergoing multiple scattering in the weak localization regime. The particular
13 scheme used is not optimum for large orders of multiple scattering, as the amount of
14 multiple scattering is limited to at most several orders by the low optical depth on
15 the relevant probe transitions, and by spontaneous emission into dark states which
16 are only weakly coupled by either the control or probe field. In the experiments
17 reported here we compare measured and theoretical polarization dependent forward
18 and sideways scattered light. Finally we note that in these studies we do not use
19 relative phase locked pump and control fields, thus realizing quite a bit shorter, and
20 more readily measurable, time scales for the time evolution of both the probe and
21 control field polarized fluorescence, and the forward scattered light.

22 In the remaining sections, we first describe the experimental approach. This is
23 followed by a presentation of our investigation of the forward scattered probe light
24 and the light polarization dependence of the scattered light in a ninety degree
25 fluorescence geometry. Comparison and discussion is made through theoretical
26 results^{32–34} obtained for a model of the experimental configurations.

27 2.1.2. Experimental Configuration

28 The sample of cold ⁸⁷Rb gas is obtained by cooling and loading the atomic vapor into
29 a magneto optical trap (MOT),³⁵ which operates near the closed hyperfine transition
30 $F = 2 \rightarrow F' = 3$. The trapping laser is derived from an external-cavity diode laser
31 (ECDL) system in a master-slave configuration, and is split into three pairs of retro
32 reflected beams, delivering an estimated trapping laser intensity of $\simeq 40$ mW/cm².
33 To prevent optical pumping of the atomic vapor into the lower energy $F = 1$
34 hyperfine level, a repumper laser is set to the $F = 1 \rightarrow F' = 2$ hyperfine transition.
35 The trap and repumper lasers can be frequency tuned and switched on or off through
36 acousto optical modulators (AOM). Fluorescence imaging measurements show that
37 the sample has an effective Gaussian atom distribution, which can be described by
 $\rho(r) = \rho_o e^{-r^2/2r_o^2}$; for this sample $r_o \approx 0.3$ mm. The temperature of the ⁸⁷Rb

1 atomic gas was determined via ballistic expansion measurements, and is estimated
 2 to be $\leq 100 \mu\text{K}$. Finally, a maximum optical depth of $b \sim 10$ on the trapping
 3 transition was determined through absorption imaging measurements, resulting in
 4 a peak atomic density of $\rho_o \sim 9 \cdot 10^{10} \text{ atoms/cm}^3$.

5 In this experiment, several overlapping Zeeman Λ schemes operating within a
 6 three energy-level configuration are shown in Fig. 1. There the resonance transition
 7 frequencies are given by f_{11} for the $F = 1 \rightarrow F' = 1$ transition, and f_{21} for the
 8 $F = 2 \rightarrow F' = 1$ transition. Before any measurement, the repumper laser is turned
 9 off for 1 ms, and in this period approximately 86% of the atoms are optically pumped
 10 to the $F = 1$ hyperfine ground state. Initially, an intense linearly polarized control
 11 laser beam with Rabi frequency Ω_c couples on bare atomic resonance the $F = 2$
 12 ground state to the $F' = 1$ excited state ($\Delta_c = 0$, where $\Delta_c = f_c - f_{21}$ is the control
 13 field detuning from resonance). The medium is then probed by a weak pulse with
 14 orthogonal linear polarization and Rabi frequency Ω_p , with a frequency detuning
 15 from the bare atomic resonance given by Δ_p . Here $\Delta_p = f_p - f_{11}$.

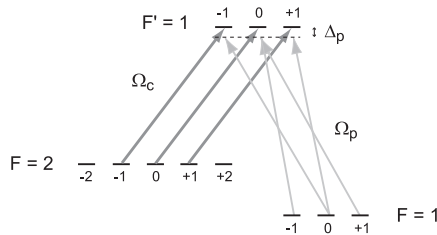


Fig. 1. Relevant hyperfine lambda scheme. The near-resonant strongcoupling laser has Rabi frequency Ω_c . The probe laser has Rabi frequency Ω_p , and detuning from the bare atomic resonance of Δ_p .

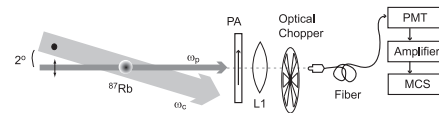


Fig. 2. Experimental setup for detection of transmission of a probe pulse through the atomic gas. The coupling laser has a frequency f_c , while the probe laser has a frequency f_p . A lens L1 collects the probe pulse transmitted through the Rb cloud and launches the beam into a fiber. PA is a polarization analyzer, PMT is a photomultiplier tube, and MCS is a multichannel scaler.

16 The control and probe lasers come from separate ECDL systems, with a com-
 17 bined root-mean-square bandwidth of 1.3 MHz, determined via optical heterodyning
 18 measurements. The control beam has a Gaussian spatial intensity profile, with a
 19 radius of $r_{\omega_c} = 0.9 \text{ mm}$, and is closely uniform in intensity over the volume of the
 20 MOT. The probe beam also has a Gaussian spatial intensity profile, and a radius
 21 of $r_{\omega_p} = 0.2 \text{ mm}$. The probe is directed through the central region of the atomic
 22 sample.

1 2.1.3. Results and Discussion

2 In this section we first present our results for forward scattering geometry, where we
 3 study the time-dependent optical behavior of a near resonance probe pulse transmit-
 4 ted through a ^{87}Rb vapor cloud dressed by an optical control field. This is followed
 5 by time-resolved observation of the polarized probe and control field induced sample
 6 fluorescence in a 90° geometry.

7 2.1.4. Forward Scattering Geometry

8 A schematic setup for the detection of the transmitted probe pulse is shown in
 9 Fig. 2. A coupling laser with frequency f_c together with a probe laser of frequency
 10 f_p forms a coupled set of near-resonance lambda configurations, and the forward
 11 scattered probe light is detected. To minimize background and to avoid saturation
 12 of the detector, the coupling laser has been offset by about 2° from the probe
 13 pulse propagation axis. A polarization analyzer (PA) selects light with the same
 14 polarization as the incident probe pulse, thus strongly suppressing the control field
 15 background at the detector. A lens L1 focuses the transmitted light into a multi-
 16 mode fiber which further directs the light to an infrared-sensitive photomultiplier
 17 tube (PMT). The time-resolved signals are then amplified using a fast preamplifier
 18 and recorded by a multichannel scaler. The system time resolution is about 5 ns.

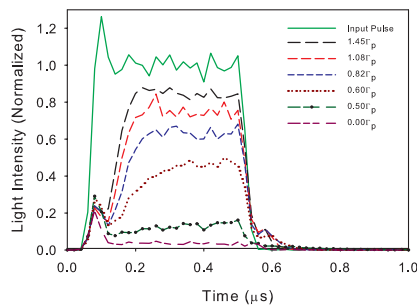


Fig. 3. Measurement of the time evolution of the transmitted probe pulse for varying Ω_c . The nearly rectangular probe pulse is 500 ns long. Data is taken at $\Delta_p = \Delta_c = 0$, for an atomic sample with optical depth of $b \simeq 3$. The slow light components can be observed as well. The probe pulse in the absence of a sample, and the probe pulse when there is no coupling laser ($\Omega_c = 0.0 \Gamma_p$) are included for comparison. Here, $\Gamma_p = 3.8 \cdot 10^7 \text{ s}^{-1}$.

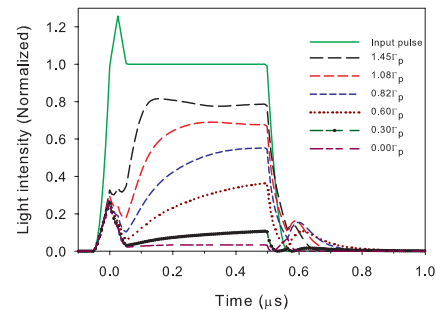


Fig. 4. Theoretical calculations of the time evolution of the transmitted probe pulse for varying Ω_c , as indicated in the caption. The probe pulse is approximately 500 ns long, at $\Delta_p = \Delta_c = 0$, for an atomic sample with optical depth of $b = 3.4$. The calculations assume a ground states decoherence rate of $0.07 \Gamma_p$. Here, $\Gamma_p = 3.8 \cdot 10^7 \text{ s}^{-1}$.

19 For a resonant optical depth of $b \simeq 3$ on the probe transition, measurements
 20 were taken to compare the time evolution and intensity of the transparency of a 500

1 ns long probe pulse as a function of the control field intensity Ω_c ; the experimental
 2 results, for a resonant probe $\Delta_p = \Delta_c = 0$, can be seen in Fig. 3. We point out
 3 that, strictly speaking this detuning relation does not precisely define the point of
 4 maximal transparency because of the additional light shift induced by the coupling
 5 with other upper-state hyperfine sublevels.³⁶ However in the discussed experimental
 6 conditions, when the Rabi frequency has the same order as the natural decay rate
 7 $\Gamma_p = 3.8 \cdot 10^7 s^{-1}$ this correction is very small. The measurements are time averaged
 8 so as to have a 20 ns time resolution; this improves the signal to noise ratio, while
 9 at the same time giving a temporal resolution shorter than the natural lifetime of
 10 26 ns. Clearly, the transparency develops for all employed values the coupling field
 11 strength, but it reaches a steady state faster for greater values of Ω_c . In these data
 12 the delayed pulses associated with slow light can be seen as well. It should be noted
 13 that the incident probe pulse is not exactly temporally square; it has an estimated
 14 rise and fall time of 40 ns. The pulse initially overshoots (about 10% above the main
 15 signal), this is due in part to initial overshooting of the acousto-optic modulator
 16 (AOM) that controls the switching of the pulse. This overshoot does not take place
 17 when the AOM switches off.

18 Theoretical calculations for the transmission of the probe pulse under similar
 19 conditions are presented in Fig. 4. The calculational approach we have used is
 20 presented in detail in several of our earlier papers,³²⁻³⁴ and is not reiterated here.
 21 We do point out that the probe pulse shape, including the mentioned overshoot,
 22 and the measured rise and fall times, is built into the calculation. In comparing
 23 Figs. 3 and 4, we see overall qualitative agreement between the experimental and
 24 theoretical time responses at the various control field Rabi frequencies.

25 From results similar to those of Fig. 3, the steady state response of the configura-
 26 tion as a function of the control field Rabi frequency may be extracted. Figure 5
 27 shows such results for Rabi frequencies Ω_c ranging from well smaller than the natu-
 28 ral width up to about 8 MHz. For this figure, the signals have been normalized such
 29 that the steady-state intensity of the incident probe pulse corresponds to 1 (100%
 30 transparency). The uncertainty in the data comes primarily from signal counting
 31 statistics and from run-to-run variations in experimental conditions.

32 Figure 6(a) presents a set of measurements taken, for a control field Rabi fre-
 33 quency $\Omega_c = 1.45 \Gamma_p$, to investigate storage and retrieval of light pulses. For
 34 these measurements the control and probe fields are simultaneously turned off (at
 35 $t = 0.6 \mu s$), and the control field is switched back on after some variable time delay.
 36 As can be seen, when the control field is turned back on, some portion of the stored
 37 light pulse is retrieved. Figure 6(b) is a plot of the integrated transmission of the
 38 probe pulse versus storage time. A fit to the data yields a $1/e$ decay time of the
 39 atomic coherence of 196 ns, or a decoherence rate on the order of 0.9 MHz. In
 40 order to physically understand this relatively large decoherence rate, we consider
 41 that when the pump and control fields are turned off, a dark state polariton is
 42 formed with some degree of efficiency. Once the probe and control fields are off,

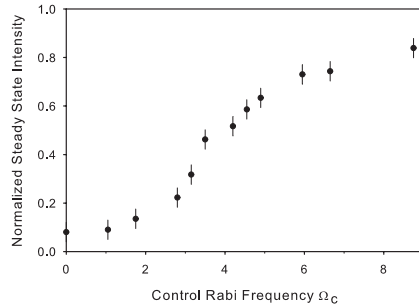


Fig. 5. Intensity of the steady-state transmitted probe signal as a function of Ω_c . The probe and control fields are on resonance ($\Delta_p = \Delta_c = 0$). The signals are normalized to the intensity of the undisturbed probe pulse.

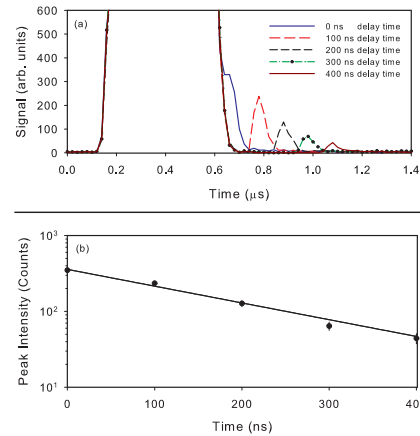


Fig. 6. Probe pulse light storage and retrieval with variable control field delays for $\Omega_c = 1.45 \Gamma_p$. (a) The control field is switched off at $t = 0.6 \mu s$, and turned on after different time intervals. (b) Comparison of the retrieved probe signal for variable storage times. A fit to the data yields a $1/e$ decay rate of the atomic coherence of 195 ns. Here, $\Gamma_p = 3.8 \cdot 10^7 s^{-1}$.

1 the quasiparticle decays relatively slowly in the dark with decoherence time limited
 2 mainly by residual magnetic fields over the volume of the atomic sample. However,
 3 when the control field is turned back on, in order to regenerate the probe optical
 4 field, the control field phase has evolved from when it was turned off. For each
 5 realization of the experiment, this phase in relation to that of the created polariton
 6 will be different. This phase evolution leads to a decay of the coherence that is
 7 proportional to the linewidth of the control laser field (~ 1 MHz), which becomes
 8 relevant when it is switched back on to regenerate the forward scattered light.

9 2.1.5. Fluorescence Detection Geometry

10 A schematic setup for the detection of fluorescence is shown in Fig. 7. In these mea-
 11 surements, the linearly polarized control laser with frequency f_c is initially switched
 12 on, and $50 \mu s$ later a weak laser probe pulse with frequency f_p and orthogonal linear
 13 polarization probes the system. A linear polarization analyzer PA selects the
 14 polarization state of the light to be detected. A lens L1 collects and collimates
 15 fluorescence coming from the location of the MOT, and a lens L2 focuses the light
 16 into a multimode optical fiber which transfers the light to the PMT. The signal is
 17 then amplified and time-resolved using a multichannel scaler. Note that for these
 18 measurements, in contrast with the transmission experiments, there is no 2° offset
 19 between the control and the probe beams. The relative response of the optical and

1 electronic detection system is calibrated for two orthogonal linear polarizations,
 2 corresponding to directions collinear with, or orthogonal to, the probe or control
 3 field. This allows meaningful measurements of the linear polarization degree of the
 4 time-resolved fluorescence to be made.

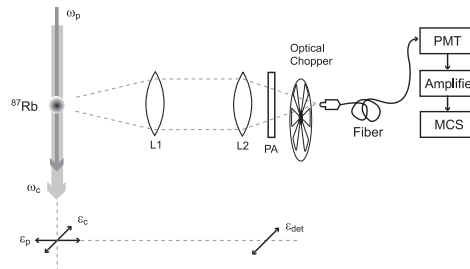


Fig. 7. Experimental setup for detection of fluorescence from a probe pulse propagating through the atomic gas. The coupling laser has a frequency ω_c . The probe laser has a frequency ω_p . A lens L1 collects fluorescence emitted from the atomic cloud, while a lens L2 focuses this light into a fiber. PA is a polarization analyzer, PMT is a photomultiplier tube, MCS is a multichannel scaler. The probe and control lasers have linear and mutually orthogonal polarization. The detected polarization is variable, and is shown in the figure to be collinear with the control field polarization. ϵ_p , ϵ_c , and ϵ_{det} are the probe, control, and detected light polarization vectors respectively. Drawing not to scale.

5 The fluorescence generated by optical excitation of the system by the probe and
 6 control fields, as a function of the control laser Rabi frequency Ω_c , is presented
 7 in Fig. 8. In these measurements the control field is linearly polarized and per-
 8 pendicular to the detector plane. The detector linear polarization analyzer is set
 9 to maximally pass light polarized in the same direction as the control field. For
 10 a control field with a low intensity ($\Omega_c < \Gamma_p$), a slower build up of fluorescence
 11 is initially observed, but the transparency is small and it has a narrow frequency
 12 width, so the main contribution to the fluorescence signal comes from scattered
 13 light having frequency components outside the transparency window. On the other
 14 hand, for large coupling field intensities ($\Omega_c > \Gamma_p$) the medium develops a high
 15 degree of transparency for a wider frequency range, which results in a suppression
 16 of fluorescence clearly observed in the data.

17 For weak control field Rabi frequencies, there is a slowly decaying portion of the
 18 fluorescence signal, as revealed by Fig. 9. To explore this slow decay, we employed
 19 a protocol like that used in storage and retrieval type of measurements of slow
 20 fluorescence light, and similar to our transmission measurements (Fig. 6). The
 21 results, for a control field Rabi frequency of $\Omega_c = 0.69 \Gamma_p$, with 5 ns resolution,
 22 are presented in Fig. 9. In these measurements, the control field was turned off
 23 at $t = 0.5 \mu s$, and switched back on with variable time delays. We see that the
 24 obtained fluorescence signals, upon switching back on the control field, with no
 25 apparent amplitude decay, for periods of time much longer than the decay time

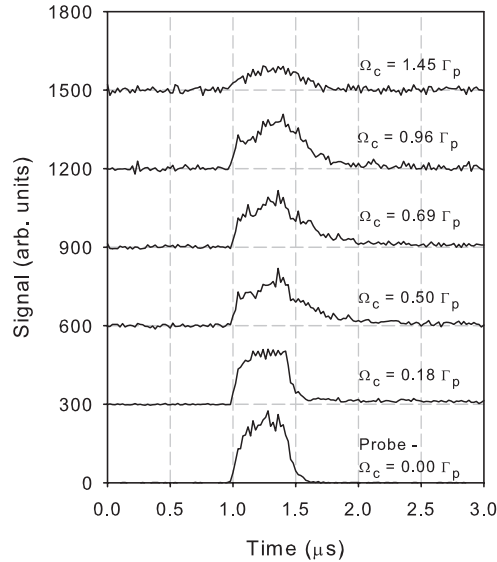


Fig. 8. Probe fluorescence from an optically dressed ^{87}Rb cloud, as a function of the control laser Rabi frequency Ω_c . The probe pulse is 500 ns long, on resonance ($\Delta_p = \Delta_c = 0$). When $\Omega_c = 0$ a characteristic probe-only fluorescence signal is detected, shown here for comparison. The control field is turned on 50 μs before the probe pulse, and stays on for 60 μs .

1 associated with the coherence time in the vapor. As we saw earlier in this section,
 2 the $1/e$ decay rate for the transmission measurements is about 200 ns. Although
 3 there is a qualitative change in the shape of the generated fluorescence pulse on
 4 the time scale of 200 ns, the persistence of the main features of this signal, which
 5 may be generated for delay times greater than 10 μs , has a different origin. We
 6 attribute these fluorescence signals to optical pumping by the control field (initiated
 7 by spontaneous Raman scattering from the $F = 1$ level), which populates the $F =$
 8 2 , $m = \pm 2$ Zeeman levels (see Fig. 1). The control beam has $\sim 0.1\%$ of light linearly
 9 polarized orthogonal to the main beam, which is enough to slowly optically pump
 10 the atoms into the $F = 2$ level, and to also contribute to the fluorescence signal in
 11 the process. For the highest control field Rabi frequencies, optical pumping occurs
 12 more quickly, and this parasitic signal, although the mechanism remains active, is
 13 not apparent in the data taken here. Such effects may occur in other circumstances,
 14 and can occur even under the circumstances when there is a high degree of phase
 15 coherence between the control field and the probe field.

16 We now turn to measurements of the polarization dependence of the time-
 17 resolved fluorescence, using the geometry of Fig. 7. For comparison purposes, we
 18 point out that we have previously reported linear polarization measurements for the
 19 case of a weak probe beam only.³⁷ In these measurements, as in the others reported

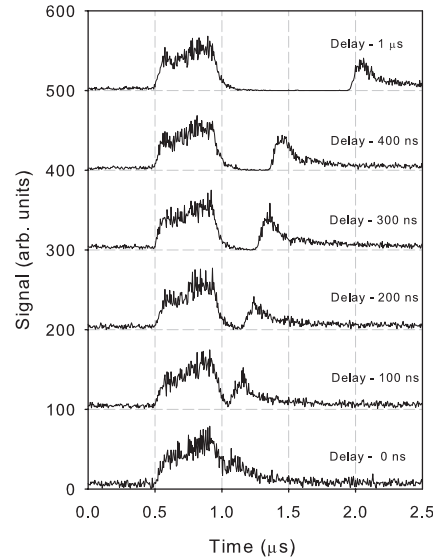


Fig. 9. Probe fluorescence as the control field, with a Rabi frequency of $\Omega_c = 0.69 \Gamma_p$, is turned off/on for various time delays. The probe pulse frequency is on resonance ($\Delta_p = 0$). The slowly decaying signal obtained when the control field is switched back on could be the result of optical pumping of atoms into the $F = 1$ level by the control field. Here, $\Gamma_p = 3.8 \cdot 10^7 \text{ s}^{-1}$.

1 in this paper, the probe and control field have mutually orthogonal linear polariza-
 2 tion directions. In the fluorescence detection arm there is a linear polarization
 3 analyzer which may be rotated so as to change the detected state of polarization.
 4 The detection plane, formed by the wave vectors of the probe and control fields, and
 5 the detected fluorescence direction, is horizontal. Four different measurements are
 6 made. In two of them, the probe field is vertical, the control field polarization vector
 7 is in the detection plane, and measurements are made of the fluorescence signals
 8 with the detector polarization analyzer either collinear with the probe field direction
 9 or perpendicular to it. In the other two measurements, the control field polarization
 10 is vertical, and the probe field vector lies in the detection plane. Again, measure-
 11 ments are made of the fluorescence signals alternately with the detector polarization
 12 analyzer collinear with the control field direction and perpendicular to it. These
 13 polarization configurations are illustrated by inserts to Figs. 10–13.

14 The measured time-resolved fluorescence signals with the *probe field* vertically
 15 polarized, and for two orthogonal states of detected light linear polarization, are
 16 shown in Fig. 10. In these measurements the data, taken in 5 ns bins, are regrouped
 17 into 20 ns bins in order to improve the signal to noise ratio. In the figure, the over-
 18 all evolution of the intensity is a rise (with an overshoot, as discussed previously)
 19 to an approximate steady state followed by decay of the signal after the probe is
 20 extinguished. We also see that the fluorescence has a nonzero degree of linear polar-
 21 ization, with an average linear polarization degree in the range 30–35%, while the

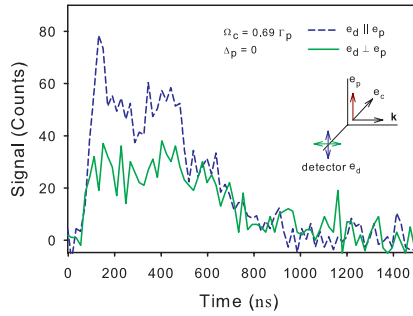


Fig. 10. Experimental results for the time-dependent polarized fluorescence under similar conditions. For these results the probe linear polarization is vertical while the control field linear polarization is horizontal. As indicated, two results are shown; in one case the linear polarization of the detected light is in the same direction as the probe linear polarization, while in the other they are orthogonal.

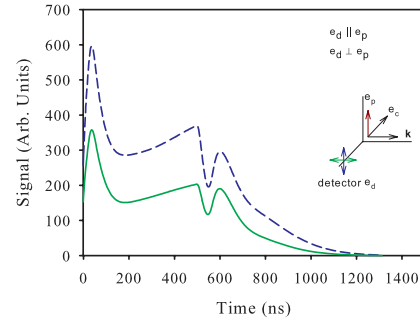


Fig. 11. Theoretical calculations of the time-dependent polarized fluorescence under similar conditions. For these results the probe linear polarization is vertical while the control field linear polarization is horizontal. As indicated, two results are shown; in one case the linear polarization of the detected light is in the same direction as the probe linear polarization, while in the other they are orthogonal.

1 probe and control field are both on. Here, as is customary, the linear polarization
 2 degree is defined as the difference in the measured intensities for the two orthogonal
 3 polarization states, normalized to the sum of these intensities. We first note that
 4 if this excitation were purely from the probe $F = 1 \rightarrow F' = 1 \rightarrow F = 1$ transition,
 5 then the linear polarization degree would be about 33%, well within the uncertainty
 6 of the measured polarization as in Fig. 10. We point out that if we include contri-
 7 bution from the spectrally unresolved $F = 1 \rightarrow F' = 1 \rightarrow F = 2$ Raman transition,
 8 the linear polarization would be reduced to $3/11$ ($\sim 27\%$). In Fig. 11 we present
 9 theoretical calculations of the time resolved fluorescence. The results are calculated
 10 for the same control field Rabi frequency as the experimental data; the relative con-
 11 trol and probe beam sizes are also matched to the experimental results. We see in
 12 the theoretical results good correspondence with respect to the measurements when
 13 the probe field remains on. However, once the field is extinguished the experimen-
 14 tal results show that the remaining transient fluorescence signals are unpolarized,
 15 within the experimental uncertainty, whereas there remains a clear polarized com-
 16 ponent in the theoretical results. We can understand these results by considering
 17 that the fluorescence signals must arise from components of the probe field that do
 18 not spectrally overlap the transparency window. With reference to Fig. 5, for the
 19 selected control field Rabi frequency of $\Omega_c = 0.69 \Gamma_p$, a significant fraction of the
 20 probe field satisfies this condition. This signal would be expected to have a linear
 21 polarization degree close to the estimates provided above for single atom scattering.

22 The measured time-resolved fluorescence signals with the *control field* vertically
 23 polarized, and for two orthogonal states of detected light linear polarization, are

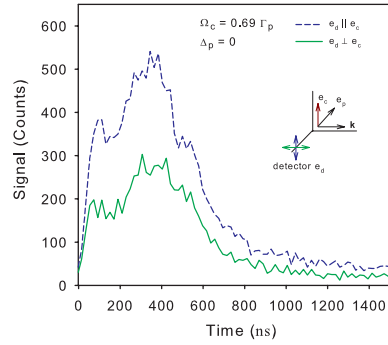


Fig. 12. Experimental results for the time-dependent polarized fluorescence under similar conditions. For these results the control field linear polarization is vertical while the probe field linear polarization is horizontal. As indicated, two results are shown; in one case the linear polarization of the detected light is in the same direction as the control field linear polarization, while in the other they are orthogonal.

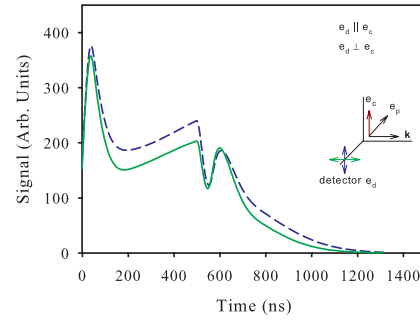


Fig. 13. Theoretical calculations of the time-dependent polarized fluorescence under similar conditions. For these results the control field linear polarization is vertical while the probe field linear polarization is horizontal. As indicated, two results are shown; in one case the linear polarization of the detected light is in the same direction as the control field linear polarization, while in the other they are orthogonal.

1 shown in Fig. 12. As for the data in Fig. 10, the time resolution is limited by the
 2 bin size of 20 ns. In the figure, the overall evolution of the experimental intensity
 3 is more structured than in the previous case. We also see that the fluorescence is
 4 linearly polarized over the entire time evolution of the signals, even after the probe
 5 and control fields are shut off; for the whole span of the data, the average linear
 6 polarization degree is about 35%. Theoretical results are calculated for the same
 7 control field Rabi frequency as the experimental data; the relative control and probe
 8 beam sizes are also matched to the experimental results. As in Fig. 11, we see in
 9 Figure 13 that the theoretical results have a qualitative correspondence with respect
 10 to the measurements. In contrast to the results of Fig. 10 and Fig. 11, we observe
 11 in Figs. 12–13 that the experimental and theoretical polarization of the fluores-
 12 cence signals are quite closely matched, even when the probe and control fields are
 13 turned off.

14 2.1.6. Conclusion

15 In this section, we have discussed several aspects of near resonance lambda scheme
 16 optical excitation of a cold sample of ^{87}Rb atoms. Forward scattering measurements
 17 are used to characterize the optical response of the dressed atomic sample. Further
 18 experiments in a right angle fluorescence geometry explore the linear polarization
 19 degree of scattered light for two different spatial configurations of the pump and
 20 control fields with respect to the fluorescence detector. These measurements show
 21 a significant linear polarization degree that is essentially constant while the probe

1 and control fields are both incident on the atomic sample. Once the fields are extin-
 2 guished the initial polarization degree of the polarized probe fluorescence rapidly
 3 decays to zero, while that of the polarized control field fluorescence is maintained.
 4 These dynamical polarization effects are in reasonable agreement with theoretical
 5 modeling of the processes.

6 **2.2. A High-Density Optical Atomic Trap for Study of Cooperative** 7 **Interactions in Light Scattering**

8 2.2.1. Brief Introduction

9 In this portion of the chapter, we give an overview of how we produce a quasi one
 10 dimensional configuration of high density and cold ^{87}Rb . Our approach builds on
 11 earlier work associated with a CO_2 laser based quasioleostatic trap.^{38,39} This
 12 modified trap may be used for a number of experiments including measurement
 13 of the forward coherent and incoherently scattered light, and experiments directed
 14 towards Anderson Localization of light in quasi one dimension. Here we focus on
 15 how we characterize the atomic sample, and illustrate with one method how a quasi
 16 one dimensional geometry can be created.

17 2.2.2. The Magneto Optical Trap

18 We begin with atoms collected and cooled in a magneto optical trap (MOT) well
 19 described by a density distribution $n(r)$ having a peak density n_0 and radius r_0
 20 given by

$$n(r) = n_0 \exp\left(-\frac{r^2}{2r_0^2}\right). \quad (1)$$

21 In order to measure the number of atoms in the MOT, we determine the absorp-
 22 tion of light from a near-resonance probe beam with intensity I_0 that is incident on
 23 the sample. From the Beer-Lambert Law, the transmitted light through the sample
 24 is

$$I_T = I_0 e^{-b}, \quad (2)$$

25 with b being the optical depth. For a not-too-optimally deep sample

$$b(r, \delta) = \sqrt{2\pi} r_0 n(r) \sigma(\delta) \quad (3)$$

26 where

$$\sigma(\delta) = \frac{\sigma_0}{1 + \left(\frac{2\delta}{\gamma}\right)^2} \quad (4)$$

27 is the scattering cross section with a laser detuning δ from resonance; γ is the
 28 lifetime of the excited state. The expression for the cross section applies when
 29 the density is not too large, and when interatomic interactions may be ignored.

1 Initially, a charge coupled device (CCD) camera takes an image of the transverse
 2 spatial probe intensity distribution. Then, an image is taken with the atomic sample
 3 present, yielding an absorption image. After background correction, the natural log
 4 of the ratio of these two images yields

$$\ln \frac{I_T(r, \delta)}{I_0} = -b(r, \delta). \quad (5)$$

5 This image is well fit to a Gaussian curve, with the amplitude equal to the peak
 6 optical depth and the $1/e^{1/2}$ radius giving r_0 of the sample. Integrating Equation
 7 (1), we find that the total number of atoms in the MOT is

$$N_{MOT} = (2\pi)^{3/2} n_0 r_0^3 \quad (6)$$

8 Using an on-resonance probe ($\delta = 0$), substitution of Eqs. (3) and (4) into Eq.
 9 (6) yields

$$N = 2\pi \frac{r_0^2 b_0}{\sigma_0} \quad (7)$$

10

$$\sigma_0 = \frac{2F' + 1}{2F + 1} \frac{\lambda^2}{2\pi} \quad (8)$$

11 Probing the $5^2S_{1/2}, F = 2 \rightarrow 5^2P_{3/2}, F' = 3$ transition with a laser of wavelength
 12 of 780 nm, we measured that the MOT typically has $\sim 5 \cdot 10^7$ atoms.

13 2.2.3. High Density Far Off Resonance Trap; Loading and Characterization

14 In order to reach the regime of higher atomic density, the atoms collected in the
 15 MOT are partially transferred to a far off resonance trap (FORT). This trap is
 16 formed at the focus of a fiber laser beam operating around 1.06 μm and having a
 17 power of several watts. To obtain optimal loading, good spatial overlap between the
 18 FORT beam and MOT atoms must be assured. This is done by controlling a wide
 19 parameter space that includes repumper beam power and turn-off time, MOT beam
 20 detuning, FORT power and alignment, and loading time. The most important of
 21 these is repumper power during loading. It is extremely sensitive to the optimal
 22 setting due to the need to reduce radiation pressure within the MOT and the ability
 23 to pump the atoms down into the $F=1$ ground state, which has a small inelastic
 24 collisional cross-section. Typically, the repumper power is reduced to $\sim 30 \mu W$ and
 25 has a turn-off time that precedes that of the MOT beam by 3 ms to help with the
 26 pumping process to the $F=1$ state. The MOT beam is detuned to also help with the
 27 compression of the MOT atoms around the FORT beam and a detuning of $\sim 10\gamma$
 28 is generally optimum. The fiber laser that provides the FORT potential, which can
 29 be increased up to 35 W, is operated around 2 W. This power setting is sufficient
 30 as the beam is focused to $\sim 18 \mu m$ giving a trap depth of 670 μK . As referenced
 31 in Ref. 40, the FORT beam focus should be offset from the center of the MOT
 32 atoms as the best loading is achieved in the throat region of the trap. This entire

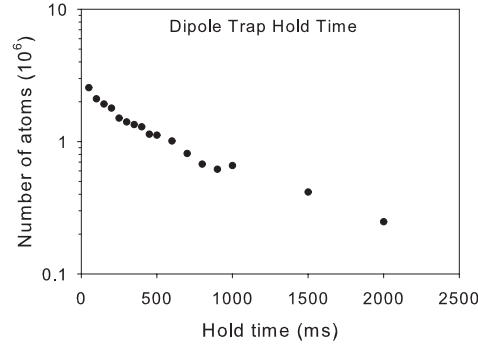


Fig. 14. Number of atoms remaining in the dipole trap as a function of time. The atom number decreases due to collisional ejection of the atoms from the trap, mainly by hot Rb atoms in the chamber.

1 experimental protocol lasts for 70 ms, typical of most FORTs,⁴¹ at which point the
 2 MOT beams are shut off along with the magnetic field and a fraction of the MOT
 3 atoms thermalize by collisions in the dipole potential trap.

4 By comparing the fluorescence of the MOT and FORT under optically thin
 5 conditions, we can then find the transfer efficiency and number of atoms successfully
 6 shifted from the MOT to the FORT. With a typical transfer efficiency of $\sim 5\%$ the
 7 FORT has $\sim 2.5 \cdot 10^6$ atoms. The number of atoms in the FORT decreases with
 8 longer hold times, as seen in Fig. 14. This is due to collisions between atoms in the
 9 FORT and background gas atoms in the vacuum chamber.

10 After finding the number of atoms in the FORT, it is necessary to know the
 11 temperature of the atom sample. The FORT has a bi-Gaussian distribution of
 12 atoms

$$n(r, z) = n_0 \exp\left(-\frac{r^2}{2r_0^2} - \frac{z^2}{2z_0^2}\right) \quad (9)$$

13 and, once thermalized, a Maxwell-Boltzmann distribution of velocities³⁵

$$f(v)d^3v = \left(\frac{2\pi k_B T}{m}\right)^{-3/2} \exp\left(-\frac{mv^2}{2k_B T}\right) d^3v. \quad (10)$$

14 Here, m is the mass of an individual atom, k_B is the Boltzmann constant, and
 15 T is the average temperature of the sample. When atoms in the FORT are released
 16 from the trap, their position will change with time according to

$$\vec{r} = \vec{r}' + \vec{v} t. \quad (11)$$

17 The time-dependent distribution of atoms, which is itself a bi-Gaussian distri-
 18 bution, is given to a good approximation by

$$n(\vec{r}, t) = \iiint_{-\infty}^{\infty} d^3v f(v) n(\vec{r} - \vec{v} t). \quad (12)$$

1 If we allow the cloud of atoms to ballistically expand, we can find the two
 2 characteristic radii of the sample as a function of time. The temperature is then
 3 proportional to the rate of change of the radii.

$$\begin{aligned} r^2 &= r_0^2 + \frac{k_B T}{m} t^2 \\ z^2 &= z_0^2 + \frac{k_B T}{m} t^2 \end{aligned} \quad (13)$$

4 The typical temperature of the FORT is $\sim 100 \mu K$ and that of our MOT is
 5 $\sim 25 \mu K$.

6 Finally, to find the initial radii of the FORT potential, and thus the effective
 7 volume, we utilize parametric resonance. Because of the low atom temperature in
 8 comparison with the trap depth, the distribution of atoms in the trap is concentrated
 9 near the bottom of the confining dipole potential. Then the radial and axial radii
 10 for the sample are significantly smaller than the beam waist and Rayleigh range,
 11 and the potential can be approximated as a harmonic oscillator

$$U(r, z) \approx -U_0 \left(1 - \left(\frac{z}{z_0^2} \right)^2 - 2 \left(\frac{r}{w_0^2} \right)^2 \right). \quad (14)$$

12 This can be rewritten to include a radial oscillation frequency ω_r and transverse
 13 frequency ω_z

$$U(r, z) = -U_0 + \frac{1}{2} m \omega_r^2 r^2 + \frac{1}{2} m \omega_z^2 z^2 \quad (15)$$

14 with harmonic oscillation frequencies of

$$\begin{aligned} \omega_r &= \sqrt{\frac{4U_0}{m\omega_0^2}} \\ \omega_z &= \sqrt{\frac{2U_0}{mz_0^2}}. \end{aligned} \quad (16)$$

15 We begin with a trapping beam with an intensity described by a Gaussian
 16 distribution, and then apply a small sinusoidal modulation to this intensity for a
 17 fixed time while the atoms are held in the potential. The strength of the modulation
 18 is h , and the frequency is ω .

$$I(r, z, t) = I(r, z) + I_0 h \cos(\omega t). \quad (17)$$

19 The one dimensional Mathieu equation describes the motion of atoms within
 20 the trap

$$\ddot{r} + \kappa \dot{r} + \omega_r^2 r (1 + h \cos(\omega t)) = 0 \quad (18)$$

21 with a relaxation rate κ . A resonance occurs when

$$\omega = 2\omega_r/n, \quad n = 1, 2, \dots \quad (19)$$

22 We can detect when we are on resonance by recording the intensity of the fluo-
 rescence as a function of frequency. The strongest response occurs at $\omega = 2\omega_r$. For

1 our FORT, the radial frequency is on the order of $2\pi \cdot 4$ kHz and the transverse fre-
 2 quency is $2\pi \cdot 45$ Hz. With these frequencies and the temperature determined from
 3 ballistic expansion, we can calculate the radial and transverse radii of the atomic
 4 sample.

$$r_0 = \sqrt{\frac{k_b T}{m\omega_r^2}}; \quad z_0 = \sqrt{2\pi} r_0 \omega_0 / \lambda \quad (20)$$

5 While the trap has a beam waist of $\sim 17.6 \mu\text{m}$ and Rayleigh range of ~ 0.92
 6 mm, the FORT atom distribution has a radial Gaussian radius of $\sim 3.4 \mu\text{m}$ and a
 7 transverse Gaussian radius of $\sim 250 \mu\text{m}$. Thus, the peak density of our sample of
 8 atoms is $6 \cdot 10^{13}$ atoms/cm³.

9 2.2.4. *Creating and Probing a Dense and Cold Quasi-One-Dimensional* 10 *Ensemble*

11 Cold atomic samples with high densities have numerous valuable and interesting
 12 properties. Our immediate interests are in three areas; (a) spectral and density
 13 dependence of the forward scattered light intensity, (b) demonstration and char-
 14 acterization of Anderson localization of light in a quasi one dimensional (Q1D)
 15 geometry, and (c) study of random lasing in Q1D. These experiments require cre-
 16 ation of a Q1D channel through the atomic sample. One way to accomplish this is
 17 described below, and an image of such a realization is shown in Fig. 15.

18 We begin with two laser beams, one near the 795 nm D1 line (the light shift
 19 (LS) laser) and one near the 780 nm D2 line (the probe). The beams are nearly spa-
 20 tially mode matched and propagate along the same axis. They are focused so that
 21 their beam waist is approximately $15 \mu\text{m}$ with a Rayleigh range of approximately
 22 $900 \mu\text{m}$. The LS laser is used to create a channel using the AC Stark shift. In

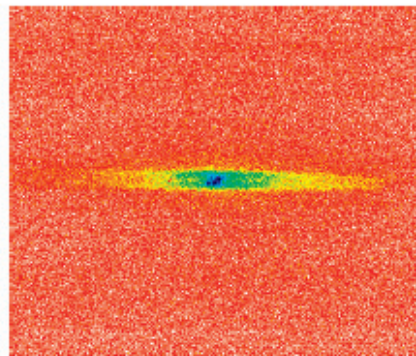


Fig. 15. Head-on image of the channel created by a laser beam traversing the center of an optical dipole trapped atom sample.

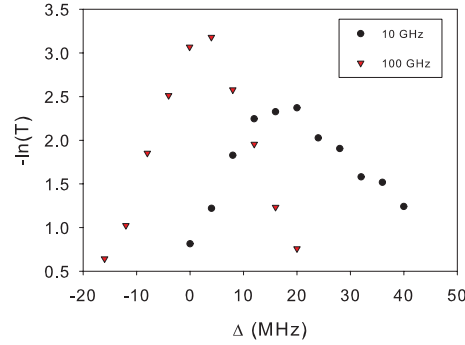


Fig. 16. Spectral shifts and Zeeman broadening of atomic resonance due to the ac Stark shift generated by the light shift laser. Data for two different detunings and a light shift laser power of about 5 mW is shown.

1 general, shifts in the ground and excited states must be considered so as to obtain
 2 the effective differential atomic resonance shift between the states. However, in
 3 performing calculations motivated by Safranova et al.⁴² and Griffin,⁴³ it was found
 4 that to a good approximation only the ground state is shifted around 795 nm. The
 5 light-shift can then be estimated as

$$\Delta E = \frac{\alpha_0 P}{\pi \epsilon_0 c w_0^2} \quad (21)$$

6 where α_0 is the scalar polarizability, P is the power of the beam, ϵ_0 is the per-
 7 mitivity of free space, c the speed of light, and w_0 the beam waist. This expression
 8 is written in SI units; division by Planck's constant h gives the shift in conventional
 9 frequency units.

10 The AC Stark shift can be measured by probing the spectral shift of hyperfine
 11 components of the D2 line. By changing the detuning or intensity of the LS laser,
 12 the ground state energy is changed, and this effect is seen by measuring the shift of
 13 resonance of the $F = 2 \rightarrow F' = 3$ transition of the D2 hyperfine multiplet. As seen
 14 in Fig. 16, detuning the LS laser 10 GHz below resonance with 5 mW of power
 15 leads to a shift of ~ 20 MHz. Increasing the detuning to 100 GHz reduces the shift
 16 by nearly a factor of 10 to 2.4 MHz.

17 Atoms within the LS beam path experience a resonance shift and the optical
 18 depth within this channel for light at the bare resonance for $5^2S_{1/2} \rightarrow 5^2P_{3/2}$
 19 is reduced. The atoms outside of this channel create a dielectric wall which is
 20 optically deep and difficult for photons to penetrate. Thus, scattering is reduced
 21 in the transverse direction and mostly limited to forwards or backwards scattering,
 22 creating a quasi-1D system.

1 2.2.5. Conclusion

2 In this chapter section, we have given an overview of one method by which to
3 create in the laboratory a quasi one dimensional configuration for light propagation
4 through a high density and cold atomic gas. We have demonstrated and partially
5 characterized such a configuration for an optical dipole trapped gas of ^{87}Rb atoms.
6 The overall scientific aim is to generate a soft cavity type arrangement for study of
7 random lasing and Anderson light localization in reduced spatial geometry.

8 Acknowledgments

9 We also appreciate financial support by the National Science Foundation (Grant
10 Nos. NSF-PHY-0654226 and NSF-PHY-1068159), the Russian Foundation for Basic
11 Research (Grant No. RFBR-CNRS 12-02-91056). D.V.K. would like to acknowledge
12 support from the External Fellowship Program of the Russian Quantum Center
13 (Ref. Number 86). We also acknowledge the generous support of the Ministry of
14 Education and Science of the Russian Federation (State Assignment 3.1446.2014K).

15 References

- 16 1. See, for example, T. Bienaime, R. Bachelard, N. Piovella and R. Kaiser, *Cooperativity*
17 *in light scattering by cold atoms*, Fortschr. Phys. 61, 377 (2013).
- 18 2. R. Friedberg, S.R. Hartmann, and J.T. Manassah, *Frequency shifts in emission and*
19 *absorption by resonant systems of two-level atoms*, Physics Reports 7, 010 (1973).
- 20 3. J.T. Manassah, *Cooperative radiation from atoms in different geometries; decay rate*
21 *and frequency shift*, Advances in Optics and Photonics 4, 108 (2012).
- 22 4. J. Keaveney, A. Sargsyan, U. Krohn, I.G. Hughes, D. Sarkisyan, and C.S. Adams,
23 *Cooperative Lamb Shift in an Atomic Vapor Layer of Nanometer Thickness*, Phys.
24 Rev. Lett. 108, 173601 (2012).
- 25 5. H. van Kampen, V.A. Sautenkov, C.J.C. Smeets, E.R. Eliel, and J.P. Woerdman,
26 *Measurement of the excitation dependence of the Lorentz local-field*, Phys. Rev. A 59,
27 271 (1999).
- 28 6. Juha Javanainen, Janne Ruostekoski, Yi Li, and Sung-Mi Yoo, *Shifts of a Resonance*
29 *Line in a Dense Atomic Sample*, Phys. Rev. Lett. 112, 113603 (2014).
- 30 7. Marlan O. Scully, *Collective Lamb Shift in Single Photon Dicke Superradiance*, Phys.
31 Rev. Lett. 102, 143601 (2009).
- 32 8. Ralf Röhlsberger, Kai Schlage, Balaram Sahoo, Sebastien Couet, and Rudolf Ruffer,
33 *Collective Lamb Shift in Single-Photon Superradiance*, Science 328, 1248 (2010).
- 34 9. R. H. Dicke, *Coherence in Spontaneous Radiation Processes*, Phys. Rev. 93, 99 (1954).
- 35 10. P.W. Anderson, *Absence of Diffusion in Certain Random Lattices*, Phys. Rev. 109,
36 1492 (1958).
- 37 11. Q. Baudouin, N. Mercadier, V. Guarrera, W. Guerin, R. Kaiser, *A cold-atom random*
38 *laser*, Nature Physics 9, 357 (2013).
- 39 12. Hui Cao, *Lasing in Disordered Media*, in Progress in Optics 45 (2003).
- 40 13. V.S. Letokhov, *Generation of light by a scattering medium with negative resonance*
41 *absorption*, Sov. Phys. JETP 16, 835-840 (1968).

- 1 14. L. V. Gerasimov, V. M. Ezhova, D. V. Kupriyanov, Q. Baudouin, W. Guerin, and R.
2 Kaiser, *Raman process under condition of radiation trapping in a disordered atomic*
3 *medium*, arXiv:1401.6641. To appear, Phys. Rev. A (2014).
- 4 15. Ping Sheng, *Introduction to Wave Scattering, Localization, and Mesoscopic Phenom-*
5 *ena* (Academic Press, San Diego, 1995).
- 6 16. Eric Akkermans and Gilles Montambaux, *Mesosopic Physics of Electrons and Pho-*
7 *tons* (Cambridge University Press, Cambridge, UK, 2007).
- 8 17. G. Labeyrie, F. de Tomasi, J.-C. Bernard, C.A. Muller, C. Miniatura, and R. Kaiser,
9 *Coherent Backscattering of Light by Cold Atoms*, Phys. Rev. Lett. 83, 5266 (1999).
- 10 18. Y. Bidet, B. Klappauf, J.C. Bernard, D. Delande, G. Labeyrie, C. Miniatura, D.
11 Wilkowski, and R. Kaiser, *Coherent backscattering of light by resonant atomic dipole*
12 *transitions*, Phys. Rev. Lett. 88, 203902-1 (2002).
- 13 19. D.V. Kupriyanov, I.M. Sokolov, N.V. Larionov, P. Kulatunga, C.I. Sukenik, and M.D.
14 Havey, *Spectral dependence of coherent backscattering of light in a narrow-resonance*
15 *atomic system*, Phys. Rev. A 69, 033801 (2004).
- 16 20. M.D. Lukin, *Trapping and manipulating photon states in atomic ensembles*, Rev. Mod.
17 Phys. 75, 457 (2003).
- 18 21. M.D. Lukin and A. Imamoglu, *Controlling photons using electromagnetically induced*
19 *transparency*, Nature 413 273 (2001).
- 20 22. T. Chaneliere, D.N. Matsukevich, S.D. Jenkins, S.-Y. Lan, T.A.B. Kennedy, and A.
21 Kuzmich, *Storage and retrieval of single photons transmitted between remote quantum*
22 *memories*, Nature 438, 833 (2005).
- 23 23. D. N. Matsukevich and A. Kuzmich, *Quantum state transfer between matter and light*,
24 Science 306, 663 (2004).
- 25 24. B. Darquie, M.P.A. Jones, J. Dingjan, J. Beugnon, S. Bergamini, Y. Sortais, G.
26 Messin, A. Browaeys, P. Grangier, *Controlled Single-Photon Emission from a Single*
27 *Trapped Two-Level Atom*, Science 309, 454 (2005).
- 28 25. S.E. Harris, J.E. Field, and A. Kasapi, *Dispersive properties of electromagnetically*
29 *induced transparency*, Phys. Rev. A 46, R29 (1992).
- 30 26. Danielle A. Braje, Vlatko Balic, G.Y. Yin and S. E. Harris, *Low-light-level nonlinear*
31 *optics with slow light*, Phys. Rev. A 68, 041801(R) (2003).
- 32 27. Danielle A. Braje, Vlatko Balic, Sunil Goda, G.Y. Yin, and S. E. Harris, *Frequency*
33 *Mixing Using Electromagnetically Induced Transparency in Cold Atoms*, Phys. Rev.
34 Lett. 93, 183601 (2004).
- 35 28. H. Kang, G. Hernandez, Y. Zhu, *Slow-light six-wave mixing at low light intensities*,
36 Phys. Rev. Lett. 93, 073601 (2004).
- 37 29. H. Kang, Y. Zhu, *Observation of large Kerr nonlinearity at low light intensities*, Phys,
38 Rev. Lett. 91, 93601 (2003).
- 39 30. D. Budker, W. Gawlik, D.F. Kimball, S.M. Rochester, V.V.Yashchuk, A. Weiss,
40 *Resonant nonlinear magneto-optical effects in atoms*, Rev. Mod. Phys. 74, 1153
41 (2002).
- 42 31. D. Budker, D.F. Kimball, S. M. Rochester, V.V. Yashchuk, *Nonlinear Magneto-optics*
43 *and Reduced Group Velocity of Light in Atomic Vapor with Slow Ground State Relax-*
44 *ation*, Phys. Rev. Lett. 83, 1767 (1999).
- 45 32. I.M. Sokolov, D.V. Kupriyanov, and M.D. Havey, *Coherent backscattering under con-*
46 *ditions of electromagnetically induced transparency*, J. Modern Optics 58, 1928 (2011).
- 47 33. V.M. Datsyuk, I.M. Sokolov, D.V. Kupriyanov, and M.D. Havey, *Diffuse light scat-*
48 *tering dynamics under conditions of electromagnetically induced transparency*, Phys.
49 Rev. A 74, 043812 (2006).

- 1 34. V.M. Datsyuk, I.M. Sokolov, D.V. Kupriyanov, and M.D. Havey, *Electromagnetically*
2 *induced optical anisotropy of an ultracold atomic medium*, Phys. Rev. A 77, 033823
3 (2008).
- 4 35. H. J. Metcalf, P. van der Straten, *Laser Cooling and Trapping*, (Springer-Verlag, New
5 York, 1999).
- 6 36. L. Giner, L. Veissier, B. Sparkes, A. S. Sheremet, A. Nicolas, O. S. Mishina, M.
7 Scherman, S. Burks, I. Shomroni, D. V. Kupriyanov, P. K. Lam, E. Giacobino, J.
8 Laurat, *Experimental investigation of the transition between Autler-Townes splitting*
9 *and electromagnetically-induced-transparency models*, Phys. Rev. A 87, 013425 (2013).
- 10 37. S. Balik, R.G. Olave, C.J. Sukenik, M.D. Havey, V. M. Datsyuk, I.M. Sokolov, and
11 D.V. Kupriyanov, *Alignment dynamics of slow light diffusion in ultracold atomic Rb*,
12 Phys. Rev. A 72, 051402(R) (2005).
- 13 38. S. Balik, A.L. Win, M.D. Havey, I.M. Sokolov and D.V. Kupriyanov, *Near-resonance*
14 *light scattering from a high-density ultracold atomic Rb gas* Phys. Rev. A 87, 053817
15 (2013).
- 16 39. A.S. Sheremet, I.M. Sokolova, D.V. Kupriyanov, S. Balik, A.L. Win and M.D. Havey,
17 *Light scattering on the $F = 1 - F' = 0$ transition in a cold and high density Rb vapor*,
18 J. Mod. Optics 61, 77 (2014).
- 19 40. S.J. Kuppens, K.L. Corwin, T.E. Chupp, and C.E. Wieman, *Loading an optical dipole*
20 *trap*, Phys. Rev. A 62, 013406 (2000).
- 21 41. M. Minarni, *Investigation of Ultracold Rb Atoms in a Pulsed Far Off Resonance Trap*,
22 Old Dominion University (2005).
- 23 42. M.S. Safranova, C.J. Williams, and Charles W. Clark, *Relativistic many-body calcu-*
24 *lations of electric-dipole matrix elements, lifetimes, and polarizabilities in rubidium*,
25 Phys. Rev. A 69, 022509 (2004).
- 26 43. Paul F. Griffin, (2005) *Laser cooling and loading of Rb into a large period, quasi-*
27 *electrostatic, optical lattice*, Durham theses, Durham University.

